

# Surface hydrogenation of vanadium dioxide nanobeam to manipulate insulator-to-metal transition using hydrogen plasma

Hyunwoo Kang, Minhwan Ko, Hyobin Choi, Wanggon Lee, Ranveer Singh, Mohit Kumar & Hyungtak Seo

To cite this article: Hyunwoo Kang, Minhwan Ko, Hyobin Choi, Wanggon Lee, Ranveer Singh, Mohit Kumar & Hyungtak Seo (2021) Surface hydrogenation of vanadium dioxide nanobeam to manipulate insulator-to-metal transition using hydrogen plasma, Journal of Asian Ceramic Societies, 9:3, 1310-1319, DOI: [10.1080/21870764.2021.1972592](https://doi.org/10.1080/21870764.2021.1972592)

To link to this article: <https://doi.org/10.1080/21870764.2021.1972592>



© 2021 The Author(s). Published by Informa UK Limited, trading as Taylor & Francis Group on behalf of The Korean Ceramic Society and The Ceramic Society of Japan.



Published online: 12 Sep 2021.



Submit your article to this journal [↗](#)



Article views: 1344



View related articles [↗](#)



View Crossmark data [↗](#)



Citing articles: 3 View citing articles [↗](#)

# Surface hydrogenation of vanadium dioxide nanobeam to manipulate insulator-to-metal transition using hydrogen plasma

Hyunwoo Kang<sup>a†</sup>, Minhwan Ko<sup>a†</sup>, Hyobin Choi<sup>a†</sup>, Wanggon Lee<sup>a</sup>, Ranveer Singh<sup>b</sup>, Mohit Kumar<sup>a,b</sup> and Hyungtak Seo<sup>a,b</sup>

<sup>a</sup>Department of Energy Systems Research, Ajou University, Suwon, Korea; <sup>b</sup>Department of Materials Science and Engineering, Ajou University, Suwon, Korea

## ABSTRACT

This report suggests the process of hydrogen doping in vanadium dioxide (VO<sub>2</sub>) nanobeam using hydrogen plasma, and in turn reveals the modification in the structural, chemical, physical, and electrical properties of VO<sub>2</sub> nanobeam that are associated with the different doping concentration. All V<sub>2</sub>O<sub>5</sub> films were grown by spin-coating followed by heat treatment for the fabrication of VO<sub>2</sub> nanobeams. Further, the hydrogen is doped using reactive ion etching process and concentration of hydrogen in VO<sub>2</sub> is controlled by power and exposure time of ion etching. The hydrogen plasma-treated VO<sub>2</sub> nanobeams exhibits an additional triclinic (T) phase in comparison to monoclinic (M1) phase (observed in the pristine) and shows a decrease in the ratio of V<sup>4+</sup> ions and forming V<sup>x+</sup> ions ( $2 \leq x \leq 3$ ). In addition, the measured work function of the VO<sub>2</sub> nanobeams decreases with increasing hydrogen doping concentration. Further, the conductivity shows increasing behavior with increasing power (etching time) for a fixed etching time (power) at room temperature and the insulator-to-metal transition (IMT) temperature was found to be decrease to  $\sim 306$  K. This study demonstrates the fine-tuning of IMT temperature just by controlling the doping concentration of hydrogen on the surface of VO<sub>2</sub> nanobeam at 300 K.

## ARTICLE HISTORY

Received 10 March 2021  
Accepted 23 August 2021



## KEYWORDS

Hydrogen doping; vanadium dioxide; nanorods; insulator–metal transition temperature; Kelvin probe force microscopy

## 1. Introduction

The nature of the phase transition in strongly correlated metal oxides (e.g. transition metal oxides) opens new possibilities for various kind of applications such as energy storage, memory storage, switching, etc. [1]. Among various metal oxides, vanadium dioxide (VO<sub>2</sub>) is of particular interest because of a variety of conceivable applications based on its ultrafast metal-to-insulator transition (MIT) [2–7]. Vanadium dioxide undergoes a first-order transition from a high-resistivity semiconductor monoclinic (M1) phase to a metallic rutile (R) phase and exhibits an effective change in electrical resistivity of the third to fourth order within a narrow temperature range [3,8–11]. This change in electrical properties is accompanied by a significant optical transition in the infrared (IR) region that exhibits thermochromic action [6,7,11–16]. The mechanism by which MIT occurs in VO<sub>2</sub> is still a debatable topic, although MIT in the VO<sub>2</sub> is generally driven by the strong electron–electron correlations associated with Mott transitions or the electron–phonon interactions associated with Peierls transitions. Consequently, much effort has been made to understand the external strain, stoichiometry, interfacial stress, and the essential effect of doping on the IMT of VO<sub>2</sub> [8–10, 16–19].

In recent years, hydrogen doping has been widely used to control the carrier concentration, electrical, and optical properties of materials [20–29]. Hydrogen acts as a powerful electron donor and, unlike other metal dopants, has a very small atomic radius, so that large distortion of the crystal lattice does not occur during the doping of hydrogen atoms in the parent materials. Therefore, excessive formation of defects, which are uncontrollable and causing degradation of MIT property, can be avoided. Thus, hydrogenation can be used in a controlled manner to manipulate electronic structures in transition metal oxides (TMO) and chalcogenide compounds to enhance their applications [30–33]. For example, Wei *et al.* have used catalytic spillover to maintain the metal state of VO<sub>2</sub> [22]. An Au film was evaporated from one end of the VO<sub>2</sub> single crystal nanobeam and then heated in a hydrogen atmosphere. Under these conditions, the Au film worked as a catalyst and the hydrogen molecules were decomposed into H atoms at the surface of the Au thin film under heating, and then H atoms were doped into the VO<sub>2</sub> nanobeam. In addition, it is demonstrated that the MIT temperature could be significantly altered by reversible doping of H atoms via low-temperature annealing using the catalytic spillover process [22]. Furthermore, Hong *et al.* have suggested the morphotropic phase transformation in

**CONTACT** Hyungtak Seo  [hseo@ajou.ac.kr](mailto:hseo@ajou.ac.kr)  Department of Energy Systems Research, Ajou University, Suwon, 16499, Korea  
†equal contribution

single-crystalline VO<sub>2</sub> nanobeams caused by thermal reduction in a hydrogen environment [23]. They demonstrated that the reduced VO<sub>2</sub> nanobeams have a non-stoichiometric composition and its lower work function exhibit a hexagonal closed packing structure, and that these properties can be correlated to the creation of the oxygen-deficiency-related defects formed in the VO<sub>2</sub> nanobeams during the reduction process.

In the present study, we have optimized H doping conditions and fabricated H doped-VO<sub>2</sub> nanobeams for the fine tuning of insulator-to-metal transition temperature in a controlled manner. In addition, the effects of H doping on the electrical and structural properties of VO<sub>2</sub> nanobeams are studied. Unlike H-doping by thermal and spillover methods, plasma H-doping has the advantage of direct doping of the reactive H<sup>+</sup> ions and H atoms at lower temperature with a fine control of the doping concentration by controlling plasma power and reaction time. Along with the optimized H-doping condition, we carefully characterized structural change, IMT temperature manipulation, and chemical/physical/electronic-property alterations of H-doped VO<sub>2</sub> nanobeams. This study provides a pathway for H-doping in the VO<sub>2</sub> nanobeam or thin films using the plasma method will be applicable for the progression of fine control of the temperature of the IMT for future optoelectronic devices.

## 2. Experimental

For the VO<sub>2</sub> nano-beam growth, thermally grown 285-nm SiO<sub>2</sub> on *p*-type Si wafers were used as a substrate, which was pre-cleaned in acetone, isopropyl alcohol (IPA), and deionized water (DI) in sequence by sonication for 5 min and dried with nitrogen. To prepare the VO<sub>2</sub> growth source, initially, 1 g of vanadium oxide (V<sub>2</sub>O<sub>5</sub>) powder (Sigma-Aldrich, Germany) was put into 20 ml of ethanol solution and then stirred at 300 K for at least 5 h. As a next step, the prepared V<sub>2</sub>O<sub>5</sub> dispersion solution (3 ml) was dropped on the substrate and spin-coated at a rate of 1000 rpm. Then, the substrate coated with V<sub>2</sub>O<sub>5</sub> solution was put on the hot plate and baked softly to remove ethanol at 340 K for a minute. Thermal chemical vapor deposition (TCVD) system (Sci&Tech Co. Ltd., Korea) was used for fabrication of VO<sub>2</sub> nanobeams using prepared V<sub>2</sub>O<sub>5</sub> powder sources. After the sample was introduced into the center of quartz tube of TCVD, the base pressure was kept at below 1 mTorr. Next, argon gas was injected in the chamber with a flow rate of 10 sccm to maintain the working pressure of 1 Torr. In addition, the growth temperature was maintained at 850°C for 2 h. After the process, the quartz tube was cooled down at 300 K by moving the heater.

Further, the reactive ion etching (RIE) equipment (Sci&Tech Co. Ltd., Korea) was used for H doping in the VO<sub>2</sub> nanobeams. The RIE system was equipped with capacitive-coupled RF power and the chamber size was 400 mm in diameter and 50 mm in height. After introducing the samples, the chamber was vacuumed to less than 9 mTorr. Thereafter, hydrogen gas was inserted into the chamber with a flow rate of 50 sccm to maintain the working pressure of 0.2 mTorr. The plasma power and etching time were varied from 10 to 100 W and 1 to 10 min, respectively, to investigate their impact on the properties of VO<sub>2</sub> nanobeams as summarized in Table 1.

To measure the electrical characteristics of the nanobeams, electrical contacts were formed by the liftoff method as follows. First, hexamethyldisilane (HDMS) and 2 μm-thick photoresist (PR) was deposited on a nanobeam-deposited sample using a spin-coater. Thereafter, using a photomask and a mask-aligner, the light of the i-line wavelength band was irradiated by 80 mJ. After soft bake, the PR in the region where the electrode pads were deposited was removed by dipping it in the developing solution. Using an electron-beam (e-beam) evaporator, 3-nm-thick titanium and 50-nm-thick gold layers were deposited on the pad for metal contacts. Finally, the remaining PR was removed using acetone. A semiconductor parameter analyzer (Keithley 4200-SCS, USA) was used to measure the electrical properties in a pressure-controllable chamber equipped with probe station. The gold/chrome electrical probe was used as a top electrode. For the temperature-dependent current–voltage measurements, a heater connected with the sample stage was used. Optical microscopy (Olympus BX51M, Japan) and field-emission scanning electron microscopy (Hitachi S-4800, Japan) were used to confirm the distribution, size, and shape of the nanobeams.

X-ray diffractometer (Rigaku Ultima III, Japan) was utilized to identify the crystal structure of the samples. In addition, transmission electron microscopy (TEM) measurements were carried out using a JEOL JEM-2100 F (USA) instrument. Selected area electron diffraction (SAED) and fast Fourier transform (FFT) were used to confirm the crystallographic plane of a films. Energy-dispersive X-ray spectroscopy (EDS) was used for the elemental analysis of the nanobeams. Further, to

**Table 1.** Plasma parameters in H<sub>2</sub> RIE doping method. Upon varying plasma-treatment time, plasma power was fixed at 50 W. Upon changing RF power, the plasma exposure time was fixed at 5 min.

Pressure (Torr)	Time (min)	RF Power (W)				
0.2	0	-	-	50	-	-
	1	-	-	50	-	-
Flow rate (sccm)	5	10	20	50	80	100
50	10	-	-	50	-	-

analyze the electronic structure of the nanobeams, X-ray photoelectron spectroscopy (XPS; Thermo Fisher Scientific Co., USA) was used. The work function of VO<sub>2</sub> nanobeams was measured by performing the Kelvin probe force microscopy (KPFM) measurements using an ex-situ atomic force microscope (NT-MDT) with conductive Pt/Ir-coated Si tip (AC240-TM), having stiffness  $\sim 0.2 \text{ Nm}^{-1}$ , diameter  $\sim 20 \text{ nm}$ , and resonance frequency  $74 \text{ kHz}$ . The time of flight-secondary ion mass spectrometry (ToF-SIMS) (ION-TOF, Germany) was used to determine the hydrogen doping depth profiles in the VO<sub>2</sub> nanobeams.

### 3. Results and discussion

#### 3.1. Growth mechanism and morphology

The VO<sub>2</sub> nanobeams are prepared from V<sub>2</sub>O<sub>5</sub> powder in a thermal chemical vapor deposition (TCVD) system, as discussed in the experimental section. The device fabrication process and schematic of final device are shown in Figure 1(a). The as-deposited VO<sub>2</sub> nanobeams are found to be crystalline in nature and have monoclinic phase, as confirmed by X-ray diffraction (XRD) and Raman spectra (Figure 2 and see supplementary Figure S1). In addition, the optical image of VO<sub>2</sub> nanobeams grown on 285 nm thick SiO<sub>2</sub> covered Si substrate is shown in Figure 1(b), confirming longitudinal growth of nanobeams in the random direction. Further, the SEM image confirms the uniform width and random distributions of the VO<sub>2</sub> nanobeams as

well as their particular shape (Figure 1(c)). Interestingly, it is found that the length and width of the nanobeams are in the range of  $50\text{--}100 \text{ }\mu\text{m}$  and  $\sim 10 \text{ }\mu\text{m}$ , respectively. Kindly note that one dimensional (i.e. height) of the nanobeams is in the range of  $200 \sim 300 \text{ nm}$ , and thus, it lies in the category of the nanosize. Based on that we judged that the expression nanobeam is appropriate to express the nanoscale in the height direction and the microscale in the length direction (Figure 1(c)). Further, for the elemental analysis, TEM-based EDS maps are carried out. Figure S2 depicts each elemental distribution of the vanadium (V), oxygen (O), and silicon (Si), respectively in different color maps. These EDS maps confirm the uniform distribution of all elements in the nanobeam along with its surface morphology.

#### 3.2. Optimization of hydrogen plasma treatment factor

##### 3.2.1. Crystal structure

It is considered that the crystallinity of films strongly depends on the doping concentration. Therefore, XRD spectra of VO<sub>2</sub> nanobeams before and after plasma treatment with different power and etching time are shown in Figure 2(a) and (b), respectively. It is observed that before plasma treatment, the (011) and (022) peaks appear at  $28^\circ$  and  $57.7^\circ$ , respectively, which are corresponding to the M1 phase of VO<sub>2</sub>. On the other hand, after H doping, the appearance of subpeaks at

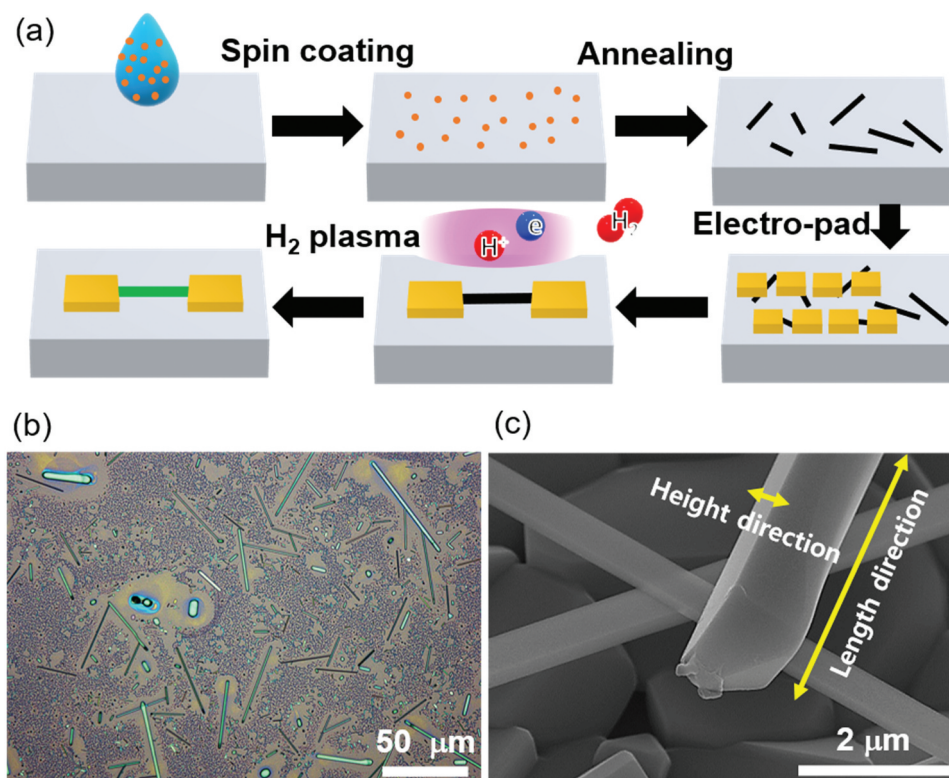


**Figure 1.** (a) Schematic illustration of VO<sub>2</sub> nanobeam device preparation process. (b) Optical microscope image of pristine VO<sub>2</sub> nanobeam. (c) SEM image of VO<sub>2</sub> nanobeam displaying typical rectangular shapes.



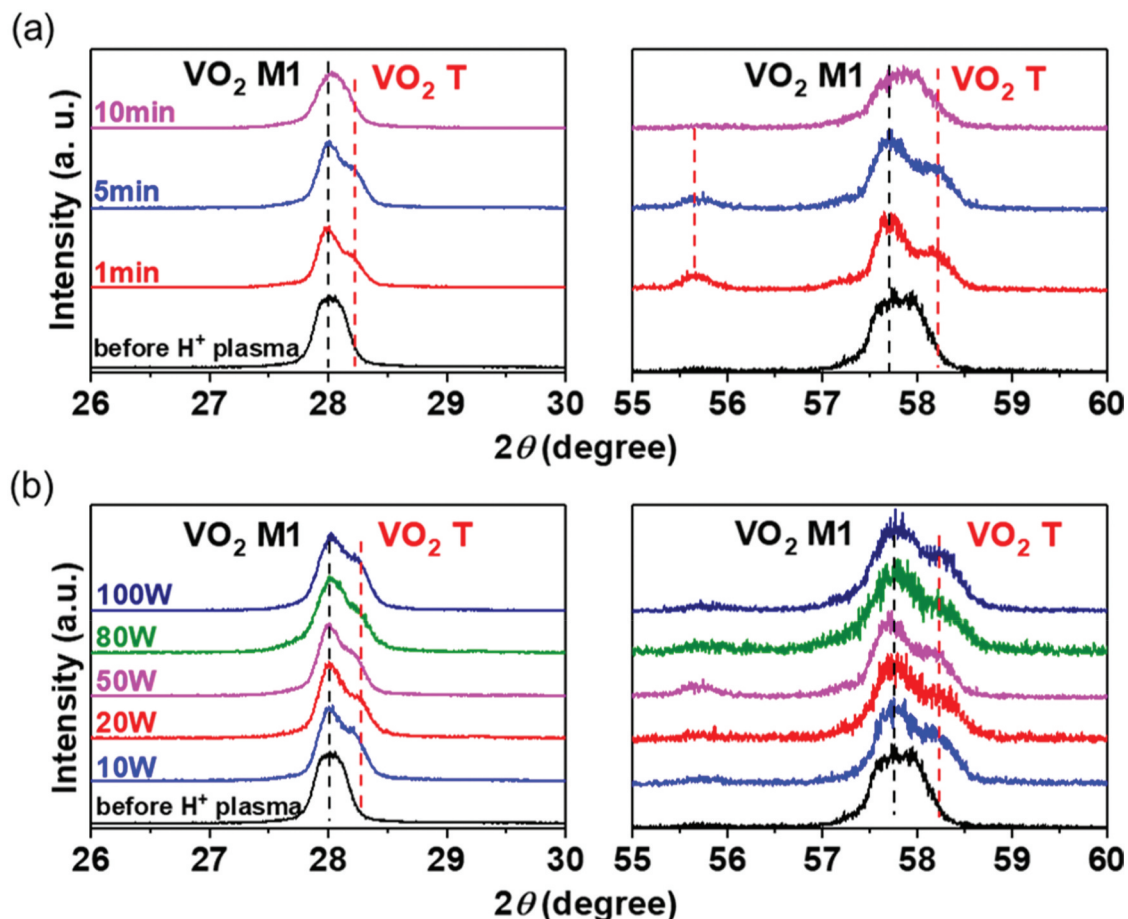


**Figure 2.** X-ray diffraction patterns for VO<sub>2</sub> nanobeam on SiO<sub>2</sub> substrate under (a) different etching time at fixed RF power and (b) different RF power at fixed etching time.

28.3° and 58.2° are observed with reduced full-width-half-maximum (FWHM) of the (011) peak for all used powers and for 1–5 min etching time. However, for 10 min etching time, the obtained XRD spectrum is found to be same as pristine sample (Figure 2(a)). It is well known that nanobeams grown in the [100] direction on a quartz substrate or an oxidized silicon substrate have a preferential orientation along (011) [22,34]. In the present case, the XRD results match well with the previous reports. In addition, no other impurities peak (for both the conditions) is observed [35] (see supplementary Figures S3 and S4). The formation of the subpeak, which seems to be derived from (011) peak, can be due to a decrease in the local (011) plane distance according to the Bragg equation. The reason behind this may be the presence of tensile stress to [100] direction and instantly compressive stress to (011) plane in the films due to H doping, which is further confirmed by Raman spectra (see supplementary Figure S1). It is reported that the Al and H doping in VO<sub>2</sub> nanobeam can introduce lattice strain due to incomplete doping and can form the triclinic (T) and/or M2 phase [22,36]. Although, in the present case, the (201) peak situated at 28.3° belongs to the T phase because in the case of the M2 phase, the

(201) and ( $\bar{2}01$ ) peaks appear simultaneously [37]. Thus, it is concluded that the formation of the subpeak is correspond to the T phase.

### 3.2.2. Electrical properties

Figure 3 represents the change in electrical properties of the VO<sub>2</sub> nanobeam with H-plasma-treatment. To study the influence of processing time and RF power on the conductivity of VO<sub>2</sub> nanobeams, ratio of conductivity increase (RCI) is calculated and compared, as shown in Figure 3(a) and b. It is interesting to note that the RCI increases from 5 to 45 with increasing RF power. With increasing RF plasma power, the reactive H<sup>+</sup> and atomic H density increase which are supplied by the active dissociation in the H<sub>2</sub> plasma. Thus, the high RF power will affect (i) the diffusion amount of the reactive H<sup>+</sup> and atomic H species from the plasma to the VO<sub>2</sub> nanobeams, (ii) the surface/bulk reaction of the VO<sub>2</sub> nanobeams associated with the adsorption and lattice bonding of hydrogen, and (iii) the lattice distortion or stress following the increase of H-doping amount. In addition, it is well known that a high intensity of plasma exposure with high RF power typically causes degradation of solid surface due to creation of oxygen vacancy and lattice distortion. On the other

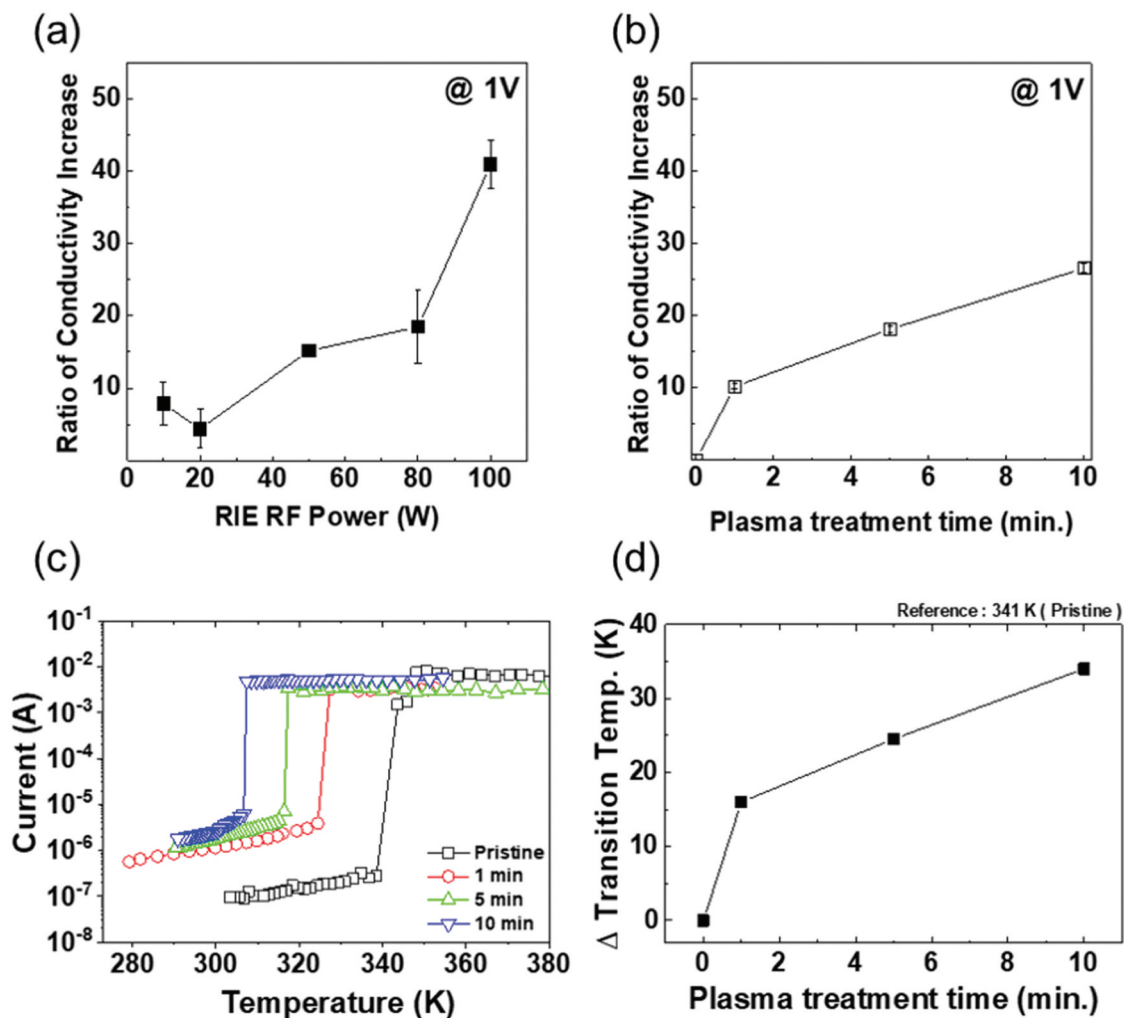


**Figure 3.** (a) The ratio of conductivity increase (RCI) dependent on RF power with fixed time at 5 min, and treatment time with fixed RF power at 50 W. (b) Temperature dependent current change of VO<sub>2</sub> nanobeam at 1 V. (c) Transition temperature difference with plasma processing time in current vs. temperature plot. (d) IMT temperature change vs. plasma treatment time.

hand, after hydrogen plasma treatment with different processing time, a relatively low deviation of 5% and a linear increase of RCI is observed, as depicted in Figure 3(b). Further, it is observed that at relatively low RF power (50 W), the steady-state condition of the diffusion and reaction of [as discussed above named (i)-(iii)] H doping at the near-surface of VO<sub>2</sub> nanobeam are mainly established up to depth of less than 10 nm (see supplementary Figure S6). In terms of device fabrication, it seems clearly that the processing time with fixed RF power of 50 W can be used for fine tuning the electrical properties of the VO<sub>2</sub> nanobeam by controlling H-doping concentration. Thus, for further electrical measurements of H-doped VO<sub>2</sub> nanobeams, the processing time and RF power of 5 min and 50 W are used as standard conditions. In addition, overall, the current level of all samples is increased by  $10 \sim 10^3$  after hydrogen doping under the plasma treatment conditions (see supplementary Figure S5).

Figure 3(c) and (d) shows the change in current in the VO<sub>2</sub> nanobeam with temperature and the degree of change in transition temperature relative to the

pristine, respectively. It is noted that the current level at insulating state increases (as shown in Figure 3(a) and (b)) and the IMT temperature also decreases proportionally to hydrogen doping time. On the other hand, the ratio of the current level at the conducting state over the insulating state is observed at  $10^4 \sim 10^5$  (as calculated from Figure 3(c)) in pristine (as calculated from Figure 3(c)) but reduced to  $\sim 10^3$  after H doping. These results definitively confirm that H doping by plasma method also modifies IMT characteristics of VO<sub>2</sub> nanobeams as found in thermal H incorporation [22].

### 3.3. Mechanism for fine tuning on the surface of VO<sub>2</sub> nanobeam

#### 3.3.1. X-ray photoelectron spectroscopy

Figure 4(a) and (b) shows the narrow scan XPS spectra of VO<sub>2</sub> nanobeams before and after H plasma treatment, respectively. The high resolution XPS spectra of V exhibits two main peaks in the range of 510–526 eV

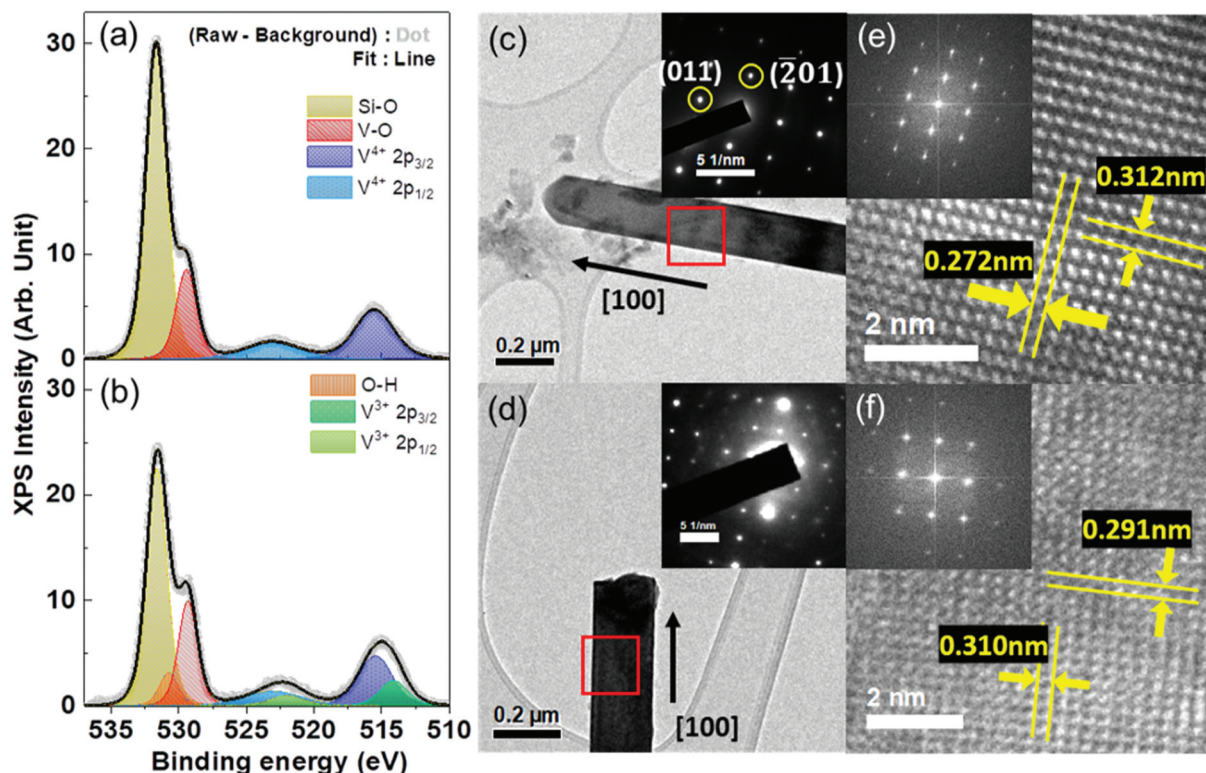


**Figure 4.** X-ray photoelectron spectrum and low-magnification bright-field TEM images; (a),(c), and (e) for pristine VO<sub>2</sub> and (b), (d), and (f) for 10 min hydrogen plasma treated VO<sub>2</sub> nanobeams. The corresponding SAED patterns are shown in the inset of each image. The zone axes are [122] for pristine VO<sub>2</sub> nanobeam. HRTEM images obtained near the edge (marked by squares) of the (e) pristine and (f) H-doped VO<sub>2</sub> nanobeams. The FFT patterns of each HRTEM image are shown in the insets.

of binding energy and no other impurity peak is observed. In the case of pristine VO<sub>2</sub> nanobeams, these two peaks are attributed to V 2p<sub>3/2</sub> and V 2p<sub>1/2</sub> at 515.5 and 523.1 eV, respectively (Figure 4(a)), which typically belong to V<sup>4+</sup> state of VO<sub>2</sub>. In addition, two distinct peaks in O 1s are observed at 529.4 and 531.7 eV, corresponding to V-O and Si-O (from substrate), respectively [34,38,39]. Due to spin-orbit coupling, the binding energy difference between V 2p<sub>3/2</sub> and V 2p<sub>1/2</sub> is found to be 7.6 eV as in previous reports [40]. On the other hand, in the V 2p narrow spectra of the hydrogen plasma-treated VO<sub>2</sub> nanobeam for 10 min (Figure 4(b)), the overall binding energy is shifted toward the lower value. In addition, upon the peak decomposition with gaussian fitting, additional peaks of V<sup>x+</sup> corresponding to 2p<sub>3/2</sub> and 2p<sub>1/2</sub> are confirmed at the binding energy of 514.1 and 522.01 eV, respectively, suggesting a presence of mixed reduced phase ( $2 \leq x \leq 3$ ) [38,39]. Also, in the O 1s spectra, O-H peak is existed at 530.74 eV, excepting for the same Si-O and V-O peaks [22,34]. The binding energy difference between V<sup>x+</sup> 2p<sub>1/2</sub> and 2p<sub>3/2</sub> due to orbital splitting is 7.91 eV. Interestingly, in heavy metals doping such as W and Mo or thermal H-doping by spillover, which have been studied to control the IMT temperature of VO<sub>2</sub>, there was no significant change in V 2p binding state [22,41]. However, from other studies, for example, Bermudez *et al.* have proposed a chemical reduction on the

surface of VO<sub>2</sub> by atomic hydrogen and reported similar kind of results in the case of hydrogen atom exposure to WO<sub>3</sub> (001) [42]. Subsequently, the same suggestion on O-H bond appearance in hydrogenated VO<sub>2</sub> was also reported [23,28,29]. These findings suggest that the reduction ratio of V<sup>4+</sup> to V<sup>x+</sup> can be directly related to V-OH bond formation. In our plasma treatment process, there were two kinds of reduction agent; the reactive H<sup>+</sup> and atom H. Especially, when active H<sup>+</sup> reacts with oxygen on the surface of VO<sub>2</sub> lattice, reduced vanadium valence can be easily formed. Also, when hydrogen atoms diffuse inside the lattice, as confirmed from XRD and Raman studies, V-O bond might be weakened by O-H, leading to a back-donation of valence electrons to V from O.

### 3.3.2 Transmission electron microscopy

Figure 4(c) and (d) represents the bright-field TEM images of the pristine VO<sub>2</sub> and 10-min H<sub>2</sub>-plasma-treated VO<sub>2</sub> nanobeams, respectively. These images confirm the uniformity of the width of nanobeams. In addition, the high-resolution TEM images of both samples, before and after H plasma treatment, are obtained near the edge [indicated by red squares in (Figure 4(b) and (c)) of the VO<sub>2</sub> nanobeams, as shown in Figure 4(e) and (f). These verifies that the nanobeams are single-crystalline and demonstrate the monoclinic crystal structure. For the pristine VO<sub>2</sub> nanobeam, the lattice spacings of the adjacent (011) and ( $\bar{2}01$ ) planes are approximately 0.312 and 0.272 nm,



respectively (Figure 4(c)) [35]. On the other hand, for the H-doped VO<sub>2</sub> nanobeams, the lattice spacings of the neighboring (011) and (201) planes are approximately 0.310 and 0.291 nm (Figure 4(f)), respectively. In addition, the change in the (011) plane distance (from 0.312 to 0.310 nm) corresponds to strain as also observed from the spectral shift to higher angles in the XRD results (Figure 2). However, for (201) plane, the change in the distance is negligible at 0.019 nm. Further, the insets in Figure 4(c–f) show the corresponding selected area electron diffraction (SAED) patterns of the TEM images for VO<sub>2</sub> nanobeams. The SAED pattern of the pristine VO<sub>2</sub> nanobeam (inset of Figure 4(c)), considered along the [1 $\bar{2}$ 2] zone axis, indicates a single-crystalline monoclinic structure with growth direction along [100]. On the other hand, the hydrogen-plasma-treated VO<sub>2</sub> nanobeams show that the nanobeams have an irregular SAED pattern suggesting the distorted crystalline structure caused by H incorporation into the VO<sub>2</sub> lattice. These measurements are in good agreement with the HRTEM results shown in the insets of panels (Figure 4(c) and (f)).

### 3.3.2. Kelvin probe force microscopy

In order to prove that hydrogen is incorporated to the surface, the KPFM measurements were performed which is very much surface sensitive technique. To reduce the variables owing to the size of the VO<sub>2</sub>

nanobeams, similar width and height of topography for all measurements are selected and measured, as shown in Figure 5(a). Figure 5(b–d) shows the contact potential difference (CPD) maps corresponding to the pristine, 5 min, and 10 min H doping VO<sub>2</sub> samples, respectively. The contact potential difference is difference between the work function of the tip and the sample. Thus, one can calculate the work function of the sample using the following equation:

$V_{\text{CPD}} = (\phi_{\text{tip}} - \phi_{\text{sample}})/e$ , where  $\phi_{\text{tip}}$  is the work function of metal tip,  $\phi_{\text{sample}}$  is the work function of a sample, and  $e$  is the electronic charge. The work function of the tip is calculated using a fresh cleaved highly oriented pyrolytic graphite (HOPG) sample. Figure 5(e) exhibits the calculated work function of VO<sub>2</sub> nanobeams for different hydrogen doping time. The work function of pristine VO<sub>2</sub> nanobeams is found to 5.39 eV, which is slightly higher than the reported value [23,43], and it decreases sequentially with increasing H-doping time. The lowest work function is found to be 5.29 eV for 10 min H doping time. From interpretation of the work function measured by KPFM from other recent studies, it has been found that the change in the work function is closely related to near-surface stoichiometry (V/O ratio related to V valence) [23] or the density of point defect like oxygen vacancy in lattice [44]. In addition, the crystal structure is also considered a factor. For example, when the work

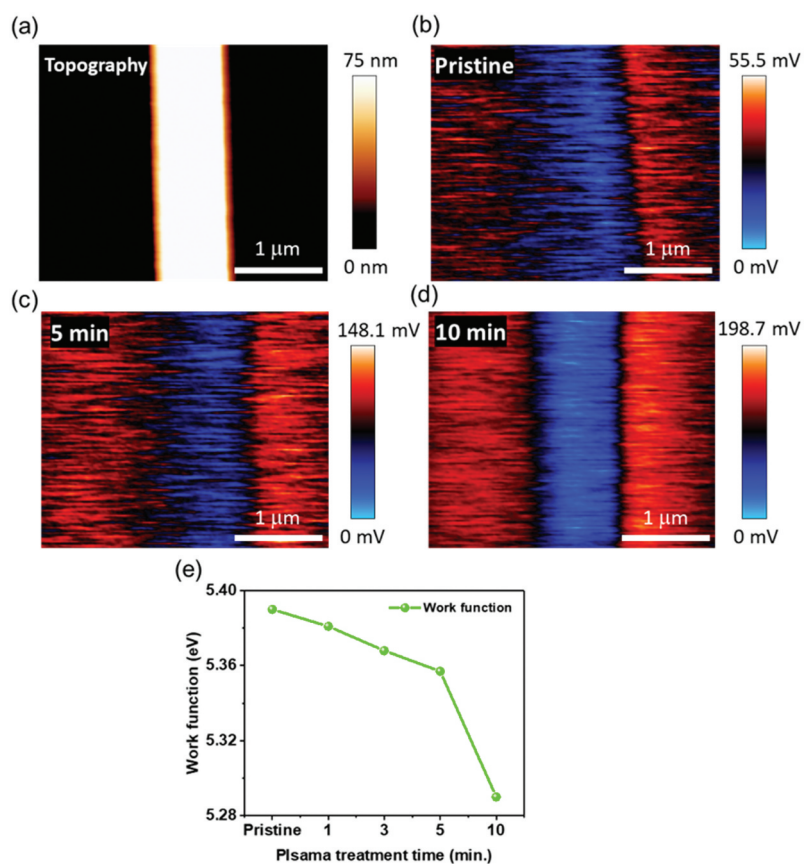
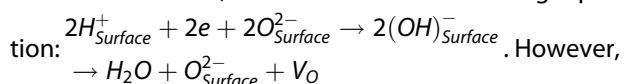


**Figure 5.** (a) Topography of pristine VO<sub>2</sub> nanobeam. (b–d) Kelvin probe force microscopy of hydrogen doped VO<sub>2</sub> nanobeam with each doping time conditions. (e) Work function deviation of the surface of VO<sub>2</sub> nanobeam with hydrogen doping time.



function of VO<sub>2</sub> nanobeam was measured in the temperature range of 300–375 K, it has been reported that the work function decreased by 0.14 eV through the transition of M1-T-M2 phase and found to be 5.16 eV in the rutile phase [45]. Among these various possible causes, based on the XPS data in Figure 4, the main factor of the decrease in work function of VO<sub>2</sub> nanobeam (in the present case) is the change in the valence state of V 2p core level toward lower binding energy (indicated as V<sup>x+</sup>), which indicates the change in the near-surface stoichiometry. Also, formation of oxygen vacancies (V<sub>O</sub>), one of the products in the hydrogenation reactions that occurs before the construction of vanadium trivalent, can be a cause like following equation:



However, in the XPS results, it is necessary to review the existence of oxygen vacancies because of the similar binding energy between Si–O and oxygen vacancy in this study.

According to the results of metal-oxide-hydrogenation studies, when hydrogen diffuses into metal oxide, the behavior of hydrogen in the oxides is found to be varying and depends on the location of the hydrogen in the lattice or the concentration of hydrogen [20,46]. This study is configured to form a steady-state hydrogen doping condition on the surface by controlling the processing time at limited RF power. Assuming that the H-doping amount increases linearly with time, when the doping amount is relatively small, a mixed phase of M1 and T is formed (as shown in Figure 2(a)) with tensile strain to [100] direction (as shown in Figure 4(b) and (e)), and at the same time, hydrogen can act as an electron donor on the surface to generate local V<sup>x+</sup> (x:1 ~ 3). As doping time is increased, the surface hydrogen concentration also increases, and when the threshold exceeds, the OH bonding located at the near-surface will be relatively weakened to form oxygen vacancies and reducing oxidation state and the strain on the (011) was relaxed. In the XPS results, the effect of surface hydrogenation was confirmed through the reduced vanadium valence and OH peak (as shown in Figure 4(d)). Through these results, it was confirmed that the largest factor influencing the transition temperature was the amount of surface V<sup>x+</sup> generated by surface hydrogenation. In addition, the results from previous studies that the transition temperature decreases in linear proportion with the concentration of the reduced V phase supports the present study [13,47].

#### 4. Conclusions

In conclusion, the effect of the hydrogen plasma doping process on the electrical properties and change in IMT temperature in the VO<sub>2</sub> single crystal nanobeam

are investigated. We successfully fabricated the H-doped VO<sub>2</sub> nanobeam by hydrogen plasma treatment in the RIE system at near 300 K. XPS studies confirm that the fractions of V<sup>4+</sup> oxidation state in the VO<sub>2</sub> nanobeams is found to be decreased. The H-doped VO<sub>2</sub> nanobeam shows an M1 and T-mixed phase as observed from the XRD and TEM results. With respect to electrical characteristics, it is shown that the current level of the H-doped VO<sub>2</sub> nanobeam increases by three orders of magnitude compared to that of the pristine sample, and the degree of increase in current was proportional to the hydrogen plasma power and treatment time. Furthermore, the IMT temperature decreases in accordance with the H plasma doping time or total amount of H in VO<sub>2</sub>. These results demonstrate that the hydrogen doping is successfully accomplished by hydrogen plasma treatment. A clear impact of H plasma doping in the reduction of vanadium oxidation state through hydrogenation over the surface of VO<sub>2</sub> nanobeam is observed, as confirmed from the surface work function of VO<sub>2</sub> nanobeam. Consequently, it is concluded that the decrease in IMT temperature is associated to amount of V<sup>x+</sup>. Overall, these results pave an efficient and viable path for the regulation of IMT temperature and electrical conductivity of the VO<sub>2</sub> nanobeam using H plasma, which is essential for the practical application of Mott-based devices.

#### Acknowledgments

This study was supported by the National Research Foundation of Korea [NRF-2019M3F3A1A03079739 and NRF-2019R1A2C2003804] of the Ministry of Science and ICT, Republic of Korea. This work was also supported by the Ajou University, South Korea.

#### Disclosure statement

No potential conflict of interest was reported by the author(s).

#### ORCID

Hyunwoo Kang  <http://orcid.org/0000-0002-7161-6940>  
Hyungtak Seo  <http://orcid.org/0000-0001-9485-6405>

#### Supporting information

Supplementary data to this article can be found online at . . .

#### References

- [1] Pierre Papon, Jacques Leblond, Paul HEM. The physics of phase transitions: concepts and applications. New York(2nd ed); 2006.
- [2] Goodenough JB. Metallic oxides. Prog Solid State Chem. 1971;5:145–399.

- [3] Imada M, Fujimori A, Tokura Y. Metal-insulator transitions. *Rev Mod Phys.* **1998**;70(4):1039.
- [4] Biermann S, Poteryaev A, Lichtenstein A, et al. Dynamical singlets and correlation-assisted peierls transition in VO<sub>2</sub>. *Phys Rev Lett.* **2005**;94(2):026404.
- [5] Hu B, Ding Y, Chen W, et al. External-strain induced insulating phase transition in VO<sub>2</sub> nanobeam and its application as flexible strain sensor. *Adv Mater.* **2010**;22(45):5134–5139.
- [6] Kasirga TS, Sun D, Park JH, et al. Photoresponse of a strongly correlated material determined by scanning photocurrent microscopy. *Nat Nanotechnol.* **2012**;7(11):723.
- [7] Bae S-H, Lee S, Koo H, et al. The memristive properties of a single VO<sub>2</sub> nanowire with switching controlled by self-heating. *Adv Mater.* **2013**;25(36):5098–5103.
- [8] Kim H-T, Chae B-G, Youn D-H, et al. Mechanism and observation of Mott transition in VO<sub>2</sub>-based two-and three-terminal devices. *New J Phys.* **2004**;6(1):52.
- [9] Stefanovich G, Pergament A, Stefanovich D. Electrical switching and Mott transition in VO<sub>2</sub>. *J Phys.* **2000**;12(41):8837.
- [10] Oka Y, Sato S, Yao T, et al. Crystal structures and transition mechanism of VO<sub>2</sub> (A). *J Solid State Chem.* **1998**;141(2):594–598.
- [11] Wentzcovitch RM, Schulz WW, Allen PB. VO<sub>2</sub>: peierls or Mott-Hubbard? A view from band theory. *Phys Rev Lett.* **1994**;72(21):3389.
- [12] Morin F. Oxides which show a metal-to-insulator transition at the Neel temperature. *Phys Rev Lett.* **1959**;3(1):34.
- [13] Schwingenschlögl U, Eyert V. The vanadium Magnéli phases V<sub>n</sub>O<sub>2n-1</sub>. *Ann Phys.* **2004**;13(9):475–510.
- [14] Liu K, Cheng C, Cheng Z, et al. Giant-amplitude, high-work density microactuators with phase transition activated nanolayer bimorphs. *Nano Lett.* **2012**;12(12):6302–6308.
- [15] Savo S, Zhou Y, Castaldi G, et al. Reconfigurable anisotropy and functional transformations with VO<sub>2</sub>-based metamaterial electric circuits. *Phys Rev B.* **2015**;91(13):134105.
- [16] Zhou Y, Ramanathan S. Mott memory and neuromorphic devices. *Proceedings of the IEEE.* **2015**;103(8):1289–1310. doi:10.1109/JPROC.2015.2431914.
- [17] Xu S, Ma H, Dai S, et al. Study on optical and electrical switching properties and phase transition mechanism of Mo 6+-oped vanadium dioxide thin films. *J Mater Sci.* **2004**;39(2):489–493.
- [18] Sohn JI, Joo HJ, Ahn D, et al. Surface-stress-induced Mott transition and nature of associated spatial phase transition in single crystalline VO<sub>2</sub> nanowires. *Nano Lett.* **2009**;9(10):3392–3397.
- [19] Wu JM, Liou LB. Room temperature photo-induced phase transitions of VO<sub>2</sub> nanodevices. *J Mater Chem.* **2011**;21(14):5499–5504.
- [20] Andreev V, Kapralova V, Klimov V. Effect of hydrogenation on the metal-semiconductor phase transition in vanadium dioxide thin films. *Phys Solid State.* **2007**;49(12):2318–2322.
- [21] Wu C, Feng F, Feng J, et al. Hydrogen-Incorporation stabilization of metallic VO<sub>2</sub>(R) phase to room temperature. displaying promising low-temperature thermoelectric effect. *J Am Chem Soc.* **2011**;133(35):13798–13801.
- [22] Wei J, Ji H, Guo W, et al. Hydrogen stabilization of metallic vanadium dioxide in single-crystal nanobeams. *Nat Nanotechnol.* **2012**;7(6):357.
- [23] Hong W-K, Park JB, Yoon J, et al. Hydrogen-induced morphotropic phase transformation of single-crystalline vanadium dioxide nanobeams. *Nano Lett.* **2013**;13(4):1822–1828.
- [24] Lin J, Ji H, Swift MW, et al. Hydrogen diffusion and stabilization in single-crystal VO<sub>2</sub> micro/nanobeams by direct atomic hydrogenation. *Nano Lett.* **2014**;14(9):5445–5451.
- [25] Warnick KH, Wang B, Pantelides ST. Hydrogen dynamics and metallic phase stabilization in VO<sub>2</sub>. *Appl Phys Lett.* **2014**;104(10):101913.
- [26] Zhao Y, Karaoglan-Bebek G, Pan X, et al. Hydrogen-doping stabilized metallic VO<sub>2</sub> (R) thin films and their application to suppress Fabry-Perot resonances in the terahertz regime. *Appl Phys Lett.* **2014**;104(24):241901.
- [27] Li Z, Guo Y, Hu Z, et al. Hydrogen treatment for superparamagnetic VO<sub>2</sub> nanowires with large room-temperature magnetoresistance. *Angew Chem.* **2016**;55(28):8018–8022.
- [28] Yoon H, Choi M, Lim T-W, et al. Reversible phase modulation and hydrogen storage in multivalent VO<sub>2</sub> epitaxial thin films. *Nat Mater.* **2016**;15(10):1113.
- [29] Chen Y, Wang Z, Chen S, et al. Non-catalytic hydrogenation of VO<sub>2</sub> in acid solution. *Nat Commun.* **2018**;9(1):818.
- [30] Kingsbury PI, Ohlsen WD, Johnson OW. Defects in Rutile. II. Diffusion of interstitial ions. *Phys Rev.* **1968**;175(3):1099–1101.
- [31] Van de Walle CG, Neugebauer J. Universal alignment of hydrogen levels in semiconductors, insulators and solutions. *Nature.* **2003**;423(6940):626–628.
- [32] Janotti A, Van de Walle CG. Hydrogen multicentre bonds. *Nat Mater.* **2006**;6(1):44.
- [33] Panayotov DA, Yates JT. Spectroscopic detection of hydrogen atom spillover from Au nanoparticles supported on TiO<sub>2</sub>: use of conduction band electrons. *J Phys Chem C.* **2007**;111(7):2959–2964.
- [34] Ko M, Lee SY, Park J, et al. Significant control of metal-insulator transition temperature through catalytic excessive oxygen doping in high-performance vanadium dioxide nanobeam channel. *J Mater Sci Technol.* **2020**;44:6.
- [35] Guiton BS, Gu Q, Prieto AL, et al. Single-crystalline vanadium dioxide nanowires with rectangular cross sections. *J Am Chem Soc.* **2005**;127(2):498–499.
- [36] Evgheni Strelcov, Alexander Tselev, Ilia Ivanov JDB, et al. Doping-based stabilization of the M2 Phase in free-standing VO<sub>2</sub> nanostructures at room temperature. *Nano Lett.* **2012**;12:8.
- [37] Armando Rúa RC, Coy H, Merced E, et al. Phase transition behavior in microcantilevers coated with M1-phase VO<sub>2</sub> and M2-phase VO<sub>2</sub>:Cr thin films. *J Appl Phys.* **2012**;111(10):104502.
- [38] Hryha ERE, Nyborg L, Nyborg L. Stoichiometric vanadium oxides studied by XPS. *Surf Interface Anal.* **2012**;44(8):4.
- [39] Mendialdua RCJ, Barbaux Y, Barbaux Y. XPS studies of V2O5, V6O13, VO<sub>2</sub> and V2O3. *J Electron Spectrosc Relat Phenom.* **1995**;71(3):13.
- [40] Hryha ERLNE, Rutqvist E, Nyborg L. Stoichiometric vanadium oxides studied by XPS. *Surf Interface Anal.* **2012**;44(8):1022–1025.
- [41] Yan Jiazhen ZY, Wanxia H, Mingjin T. Effect of Mo-W Co-doping on semiconductor-metal phase transition temperature of vanadium dioxide film. *Thin Solid Films.* **2008**;516(23):5.

- [42] Bermudez V, Williams R, Long J, et al. Photoemission study of hydrogen adsorption on vanadium dioxide near the semiconductor-metal phase transition. *Phys Rev B*. [1992](#);45(16):9266.
- [43] Rongbin Wang TK, Ke-Ke F, Zhai T, et al. Oxygen vacancies allow tuning the work function of vanadium dioxide. *Adv Mater Interfaces*. [2018](#);5(22):7.
- [44] Rongbin Wang TK, Ke-Ke F, Zhai T, et al. Oxygen vacancies allow tuning the work function of vanadium dioxide. *Adv Mater Interfaces*. [2018](#);1801033:1–7.
- [45] Changhyun ZY, Yang Z, Ramanathan SK, et al. Work function of vanadium dioxide thin films across the metal-insulator transition and the role of surface nonstoichiometry. *ACS Appl Mater Interfaces*. [2011](#);3(9):3396–3401.
- [46] Baikov YM. The chemical state and the mobility of hydrogen in oxide–hydroxide solids. *Solid State Ion*. [1997](#);97(–14):471–476.
- [47] Bugaev AAZ, Chudnovskii, F. A BP. The metal-semiconductor phase transition and its application. Leningrad, Izdatel'stvo Nauka. [1979](#);184.